A statistical study of gravity waves in the polar regions based on operational radiosonde data

Motoyoshi Yoshiki

Department of Geophysics, Faculty of Science, Kyoto University, Kyoto, Japan

Kaoru Sato

National Institute of Polar Research, Tokyo

Abstract. Gravity waves in the lower polar stratosphere are examined using operational radiosonde observations gathered from 33 stations over a period of 10 years. Both the potential and kinetic energies of the gravity waves vary annually and reach maxima in winter in the Arctic and in spring in the Antarctic. In the Antarctic spring a region of large gravity wave energy propagates downward following the movement of a zone of high static stability associated with Southern Hemispheric warming. Moreover, the enhanced energy region and the high stability zone coincide in the horizontal plane and move gradually from 135°E, 50°S to 45°W, 70°S over the South Pole. The vertical and horizontal directions of wave propagation are examined using hodograph analysis in the vertical. Most gravity waves transfer energy upward in the Arctic, while the percentage of downward energy propagation is relatively high in winter and spring in the Antarctic. Horizontally, gravity waves propagate westward relative to the mean wind in the Arctic, while in the Antarctic the dominant direction varies from station to station. The correlation between gravity wave energy in the lower stratosphere and the mean wind is also examined. In the Arctic, gravity wave energy is highly correlated with the surface wind, though in the Antarctic it correlates with the stratospheric wind. These results suggest that gravity waves observed in the Arctic are forced by topography, whereas in Antarctica some sources may exist in the stratosphere. One such source candidate is likely to be the polar night jet.

1. Introduction

Since the theoretical work of *Lindzen* [1981] and *Matsuno* [1982], numerous observational and theoretical studies have been made to examine the importance of gravity waves in the global circulation of the middle atmosphere. Momentum flux convergence is associated with dissipation of gravity waves by radiation, viscosity, and/or instability and acts on the mean wind as a force. The wave-induced force can either accelerate or decelerate the mean wind to a value approaching the wave phase velocity, but so far, the decelerative aspect of wave-induced force has tended to be emphasized in the literature. For example, gravity waves of low phase velocity are thought to maintain the weak zonal wind around the mesopause at midlatitudes. However, the accelerative aspect of gravity waves is also important, particularly in driving the quasi-biennial oscillation of the mean zonal wind in the equatorial lower stratosphere [e.g., *Dunkerton*, 1997; *Sato and Dunkerton*, 1997].

In the polar regions, gravity waves are considered to decelerate the polar jet and keep the atmosphere warm in the polar vortex. Another important and recently highlighted aspect

of gravity waves in the polar regions is their role in chemical processes, such as the formation of polar stratospheric clouds (PSCs) [*Carslaw et al.*, 1998]. Even if the temperature is above the condensation or frost point of nitric acid trihydrate (NAT) and/or water vapor on synoptic or larger scales, small-scale temperature fluctuations associated with gravity waves may cause both rapid cooling and the lower local temperatures needed for cloud formation. In many observational case studies, PSCs associated with mountain waves are investigated [e.g., *Cariolle et al.*, 1989].

Gravity wave activity in the polar region is related to the position of the stratospheric polar vortex [*Whiteway et al.*, 1997] and maximizes when the station locates at the edge of the vortex. On the other hand, minimum in wave activity is observed when the station is on the inside of the vortex. The effect of critical level filtering can be examined using data from an airborne microwave temperature profiler [*Bacmeister et al.*, 1990] and radiosondes [*Whiteway and Duck*, 1996].

In order to obtain a comprehensive understanding of dynamical and photochemical effects of gravity waves, more statistical information on their geographical distribution and seasonal variations is necessary. However, most statistical studies of gravity waves have so far concentrated on middle and low latitudes.

Using operational radiosonde observations gathered in Japan over the latitudinal range of 25°–45°N, *Kitamura and*

Hirota [1989] showed that gravity wave energy in the lower stratosphere changes annually and develops a maximum in winter. *Sato* [1994] examined the detailed characteristics of gravity waves using a mesosphere, stratosphere, and troposphere (MST) radar operating in Japan (35°N, 165°E). She found that the vertical flux of zonal momentum is negative in winter and mostly zero in summer and considered topographically forced gravity waves to be the most plausible cause of the negative momentum fluxes in winter. She also showed the dominance of gravity waves propagating equatorward above the subtropical jet in winter. In the equatorial lower stratosphere, gravity wave intensity has a dominant variation synchronized with the quasi-biennial oscillation of the mean zonal wind rather than the annual variation [*Sato et al.*, 1994; *Maruyama*, 1994]. In the Southern Hemisphere, *Allen and Vincent* [1995] examined gravity wave energy in the latitudinal range of 12°–68°S. Gravity wave energy increases monotonically toward the equator in summer, while the energy maximizes at midlatitudes in winter.

In the polar regions, there are few statistical studies. Most studies in the polar regions are from specific campaigns which have limited space-time coverage. One exception is the study by *Pfenninger et al.* [1999], who examined the characteristics of gravity waves in the lower stratosphere at the South Pole using high-resolution radiosonde data. They showed that gravity wave energy is large in spring and that the slope of the vertical wavenumber spectrum is shallower than at midlatitudes. The present study was performed independently of *Pfenninger et al.* [1999], although part of our results, such as the seasonal variation of gravity wave energy and its correspondence with atmospheric static stability, overlap (first presented at the 74th meeting of Japan Meteorological Society on October 21, 1998).

In this paper, the temporal variation, spatial distribution, and the structure of gravity waves in the polar regions of both hemispheres are examined utilizing operational radiosonde observations gathered over 10 years at many stations. In section 2, details of the radiosonde data are described. Gravity wave characteristics, such as spatial distribution, temporal variation, and wave structure, are shown in section 3. Results are discussed in section 4. Concluding remarks are given in section 5.

2. Data Description

We have analyzed data obtained by twice daily operational radiosondes operated at meteorological stations in the polar regions over a 10 year period from 1987 to 1996. These are archived and provided by National Centers for Environmental Prediction (NCEP).

Stations at latitudes higher than 40°S and 60°N which provide data of sufficient quality were selected. Data from 12 stations in the Northern Hemisphere and 21 stations in the Southern Hemisphere were chosen for use in this study. The locations of the stations are shown in Figure 1, and their names are listed in Tables 1 and 2 for Northern and Southern Hemisphere, respectively. Hereafter, the regions at latitudes higher than 60°N and than 60°S are referred to as the Arctic and the Antarctic, respectively. In the Southern Hemisphere, six midlatitude stations (shown as A, B, C, D, T, and U in Figure 1) are also included for comparison with the Antarctic stations. The Arctic stations are mostly located in the European sector.

We used both mandatory and significant levels, whose height intervals are about 1–2 km in the lower stratosphere. To maintain the fine structure present in the observations, we interpolated the temperature and wind data linearly in the vertical at the same intervals of 200 m. Log pressure coordinates are used to describe altitudes. Gravity wave components are defined here as fluctuations whose vertical wavelengths are between 2 and 8 km. We also used NCEP reanal-
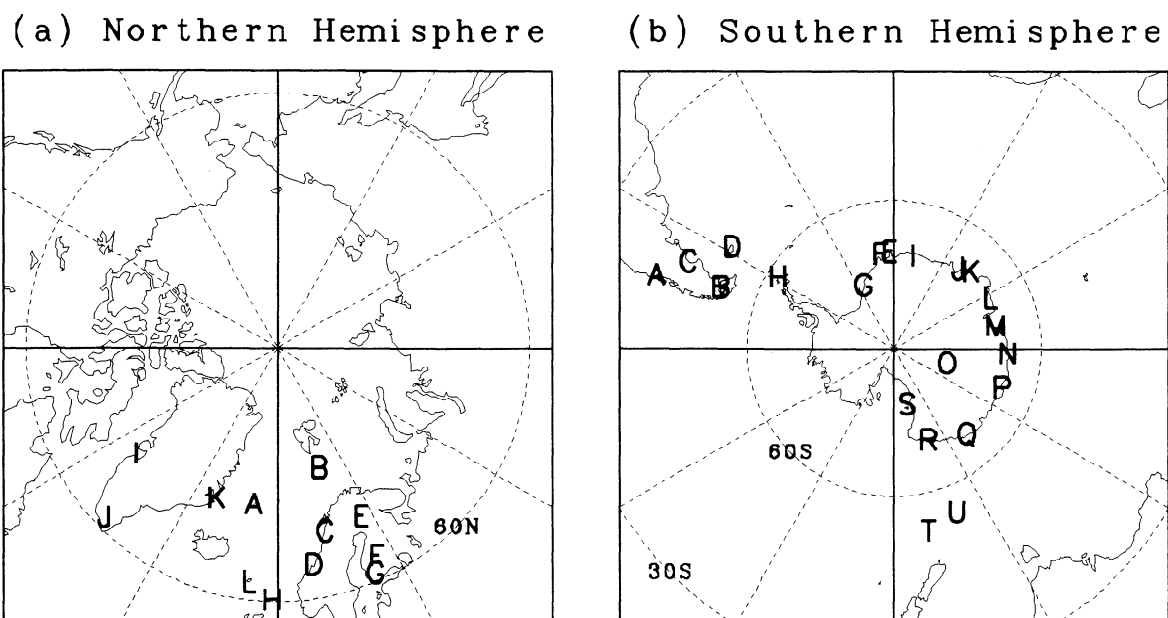
(a) Northern Hemisphere   (b) Southern Hemisphere

Figure 1. Maps of meteorological stations chosen for the analysis in this study. The stations denoted by capital letters are listed in Tables 1 and 2.
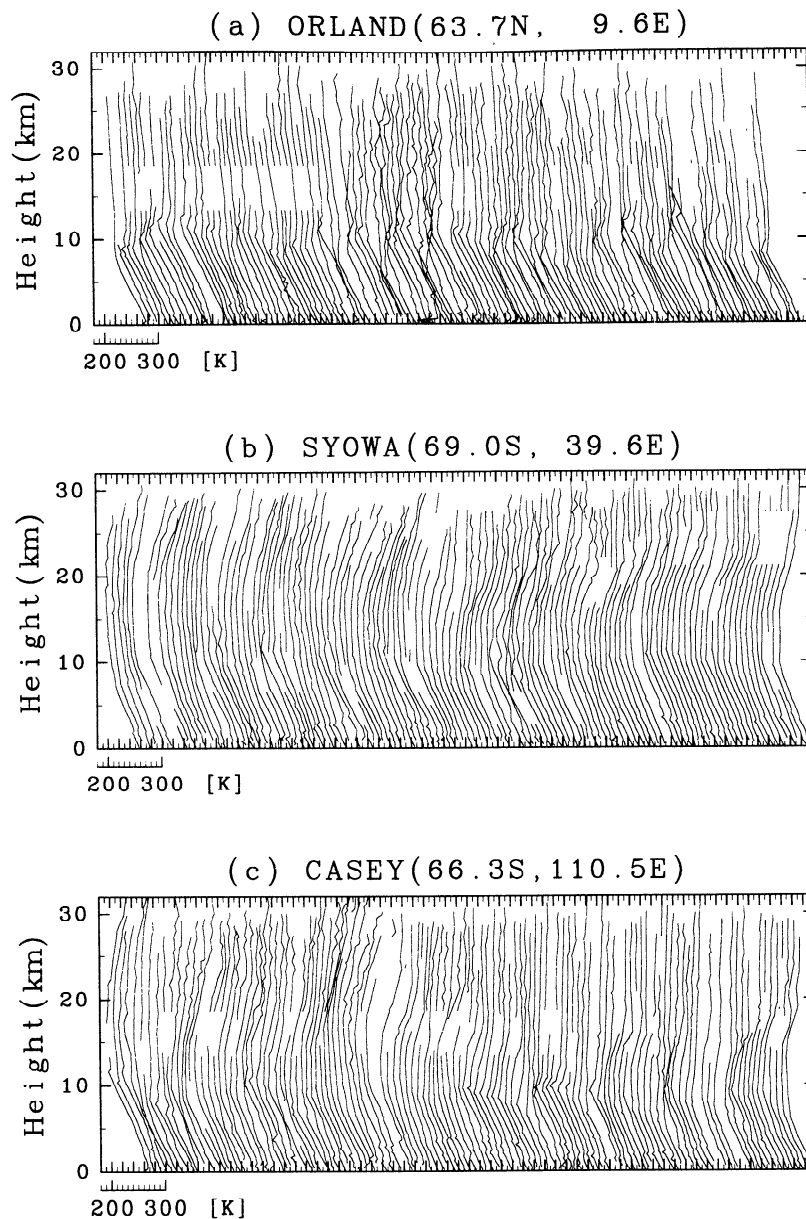
Figure 2. Time series of temperature profiles at (a) Orland (63.7°N, 9.6°E) from November 1, 1994 to December 31, 1994, and (b) Syowa (69.0°S, 39.6 °E) and (c) Casey (66.3°S, 110.5°E) from September 1, 1994, to October 31, 1994. The profiles are shifted by 10 K intervals.

ysis data over the same period to examine the background field of the gravity waves.

3. Results

Figure 2 shows the time series of the temperature profile from November 1, 1994, to December 31, 1994, at Orland (Figure 2a; shown as capital D in Figure 1a) and from September 1, 1994, to October 31, 1994, at Syowa (Figure 2b; shown as capital J in Figure 1b) and Casey (Figure 2c; shown as capital P). The profiles are shifted by an interval of 10 K. The displayed periods are selected to show gravity wave activity at each station, as is discussed later. At all stations, small-scale fluctuations having large amplitudes of 5 K can be seen in the height region of 15–30 km.

3.1. Seasonal Variation of Gravity Wave Energy in the Arctic and the Antarctic

Figure 3 shows the 10 year average of the variation of the mean square of temperature and horizontal wind components of gravity waves. These data were derived from Arctic and Antarctic stations and refer to a height region of 15–20 km in the lower stratosphere. The mean square of fluctuations was calculated for every one third of a month. Note that winter months are centered in the horizontal time axis for both time series so as to make comparison of the seasonal variation between the Arctic and the Antarctic easier.

In the Arctic both the mean squares of temperature and horizontal wind components are large in winter and small in summer at all stations. This behavior is similar to the results

Table 1. List of Meteorological Stations in the Northern Hemisphere

	Station	Latitude °North	Longitude °East	z m	Station Name
A	01001	70.93	-8.67		Jan Mayen
B	01028	74.52	19.02		Bjornoya
C	01152	67.25	14.40	20	Bodo
D	01241	63.70	9.60		Orland
E	02836	67.37	26.65	179	Sodankyla
F	02935	62.40	25.68	141	Jyvaskyla
G	02963	60.82	23.50	104	Jokioinen
H	03005	60.13	-1.18	82	Lerwick
I	04220	68.70	-52.75	43	Egedesminde
J	04270	61.15	-45.43	4	Narsarsuaq
K	04339	70.48	-21.95	65	Scoresbysund
L	06011	62.02	-6.77	54	Torshavn

for midlatitudes shown in previous studies [e.g., *Sato*, 1994; *Murayama et al.*, 1994]. In the Antarctic the seasonal variation is unique: The mean squares are maximized in spring at most stations. This feature of the Antarctic data is consistent with the result of *Pfenninger et al.* [1999] at the South Pole. It is interesting that the energy enhancement in spring is commonly seen at the Antarctic stations.

Next, time-height sections of gravity wave potential energy (PE $\equiv g^2\overline{T'^2}/N^2\overline{T^2}$) and kinetic energy (KE $\equiv \overline{u'^2 + v'^2}$) divided by air density averaged over 10 years were calculated, where g is gravitational acceleration, T is temperature, N is the Brunt-Väisälä frequency, u is zonal wind, and v is meridional wind. Overbars show an average in time, and primes denote gravity wave components defined in sec-

tion 2. Results are shown for Orland (63.7°N, 9.6°E) and Syowa (69.0°S, 39.6°E) in Figures 4 and 5, as typical examples of the Arctic and Antarctic, respectively. We ignored the contribution of the vertical wind component w to the kinetic energy because it is considered to be small.

At Orland both potential and kinetic energies are enhanced in winter in the height region of 15–25 km. In the vertical they are maximized above 26 km in winter. Another maximum is seen around 10 km, where the tropopause is located in all seasons. Although the maximum in potential energy at the tropopause may represent contamination due to the abrupt change of temperature lapse rate, the maximum observed in kinetic energy is likely to indicate large amplitude gravity waves.

Table 2. List of Meteorological Stations in the Southern Hemisphere

|	Station	Latitude °North	Longitude °East	z m	Station Name
A	85799	-41.42	-73.08	85	Puerto Montt
B	85934	-53.00	-70.85	37	Punta Arenas
C	87860	-45.78	-67.50	46	Comodoro Rivadavia Aero
D	88889	-51.82	-58.45	74	Mount Pleasant Airport
E	89001	-70.30	-2.35	62	S.A.N.A.E. Station
F	89002	-70.67	-8.25	50	Neumayer
G	89022	-75.50	-26.65	30	Halley
H	89050	-62.20	-58.93	16	Bellingshausen
I	89512	-70.77	11.83		Novolazarevskaja
J	89532	-69.00	39.58	18	Syowa
K	89542	-67.67	45.85		Molodeznaja
L	89564	-67.60	62.87	10	Mawson
M	89571	-68.58	77.97	18	Davis
N	89592	-66.55	93.02		Mirnyj
O	89606	-78.45	106.87		Vostok
P	89611	-66.28	110.52	40	Casey
Q	89642	-66.67	140.02	41	Dumont d'Urville
R	89657	-69.50	69.38		Leningradskaja
S	89664	-77.85	166.67	24	McMurdo
T	93944	-52.55	169.15		Campbell Island
U	94998	-54.48	158.95	6	Macquarie Island
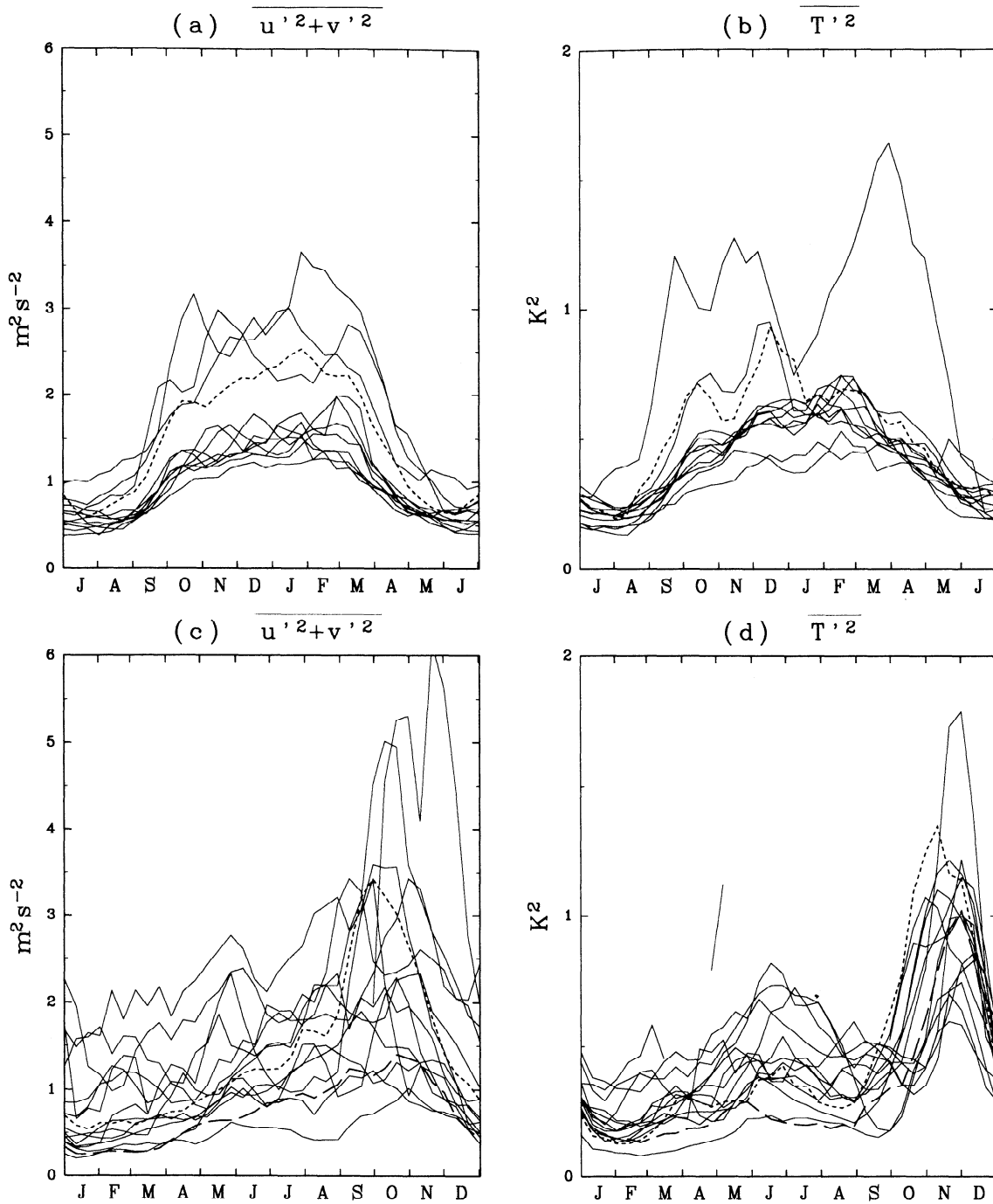
Figure 3. Seasonal variation of the mean square of temperature and horizontal wind fluctuation averaged for a height region of 15-20 km at each station in (a and b) the Arctic and (c and d) the Antarctic. The dashed curve in Figures 3a and 3b indicates the seasonal variation at Orland. The long-dashed and short-dashed curves in Figures 3c and 3d indicate those at Syowa and Casey, respectively.

At Syowa, potential and kinetic energies are maximized around 10 km in all seasons and above 26 km in winter similar to Orland. However, there is a significant difference between Syowa and Orland. At Syowa the maximum of potential energy is observed in spring in the height region of 15-26 km in the lower stratosphere. The maximum appears in early October around 26 km. The region with large potential energy propagates downward, and the maximum is observed in

late November at 17 km. A similar tendency is also seen in the kinetic energy profile.

Figures 6 and 7 show time-height sections of unfiltered zonal wind, temperature, and the Brunt-Väisälä frequency squared which are averaged over 10 years at Syowa and Orland, respectively. At Syowa the winter polar jet stays longer than that at Orland. In spring the warming occurs earlier at higher altitude in the region of 15-30 km, and hence the
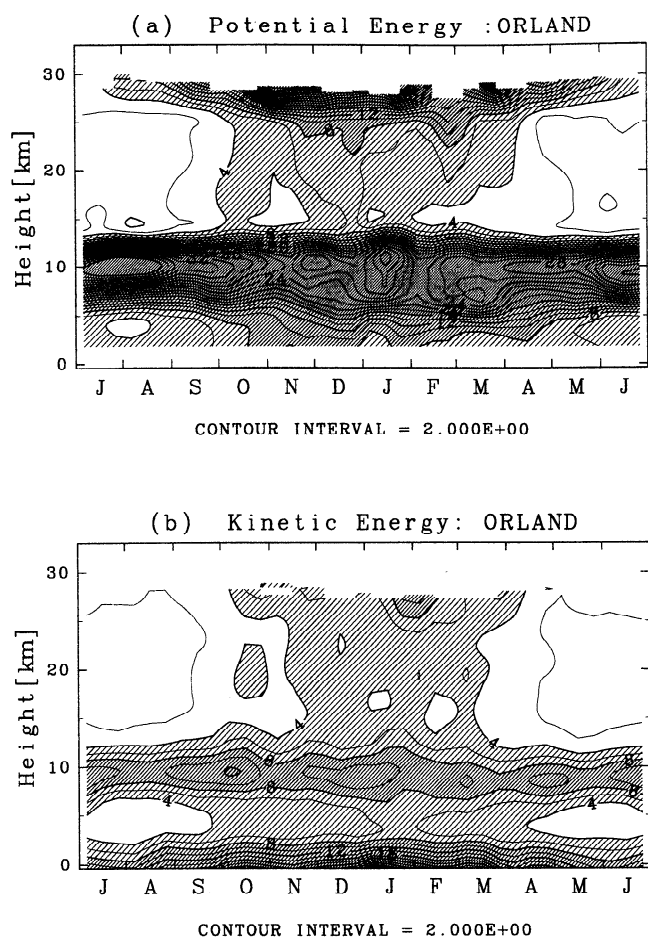
(a)   Potential Energy : ORLAND

CONTOUR INTERVAL = 2.000E+00

(b)   Kinetic Energy: ORLAND

CONTOUR INTERVAL = 2.000E+00

Figure 4. A composite of the time-height section of (a) potential and (b) kinetic energy of gravity waves at Orland (63.7°N, 9.6°E). The units are m² s⁻². The contour interval is 2 m² s⁻².

region with high static stability propagates downward. It should be noted that the maximum in the potential energy of gravity waves is observed when and where the static stability becomes high. At Orland the spring warming occurs at all levels almost simultaneously in a climatological sense, whereas enhancement of the static stability in spring (as at Syowa) is not seen.

3.2. Regional Dependence of Gravity Wave Energy Variation During the Spring Time Warming Over the Antarctic

The spring maximum of gravity wave activity is seen at most Antarctic stations (see Figures 3c and 3d) in the height region of 15–20 km. However, the gravity wave enhancement in spring does not occur simultaneously in the Antarctic. It seems that the maximum of the activity occurs earlier at Casey (the short-dashed curve) than at Syowa (the long-dashed curve), for example.

Since the first observations of the springtime warming during the International Geophysical Year (1957–1958), the difference in the seasonal march between the Southern Hemisphere and the Northern Hemisphere has been recognized. In the Southern Hemisphere the springtime warming does

not occur simultaneously over the whole area of the polar region but begins in the 135°E sector and propagates toward the South American sector gradually [*Phillpot*, 1969, 1989].

Figure 8 shows a climatology of temperature T over the same 10 years of 1987–1996 at 50 hPa (roughly corresponding to a height of 20 km) made using NCEP reanalysis data. A region of warm air appears around 90°–150°E, 50°S in September and propagates toward the direction of 45°W along a line of longitude with increasing temperature in October and November. In late December, Antarctica is fully covered by a warm air mass. This feature can be seen more clearly in the latitude-time cross section of the mean temperature averaged for the height region of 15–20 km (Figure 9). The top of the vertical axis of Figure 9 shows latitudes at 135°E and the bottom shows latitudes at 45°W. A cold core is situated around the South Pole in winter, and the temperature begins to rise in spring. The warming occurs earlier at lower latitudes at 135°E and later at latitudes at 45°W. The time lag between the locations of 135°E, 60°S and 135°E, 90°S is ~ 2 months. The transition takes ~ 1 month at each latitude.

Figure 10 shows the latitude-time section of the Brunt-Väisälä frequency squared (N^2) averaged for the height region of 15–20 km. Solid boxes denote the time when the static stability is highest at each latitude. In the midlatitude region (lower than 65°), the annual variation of N^2 is not
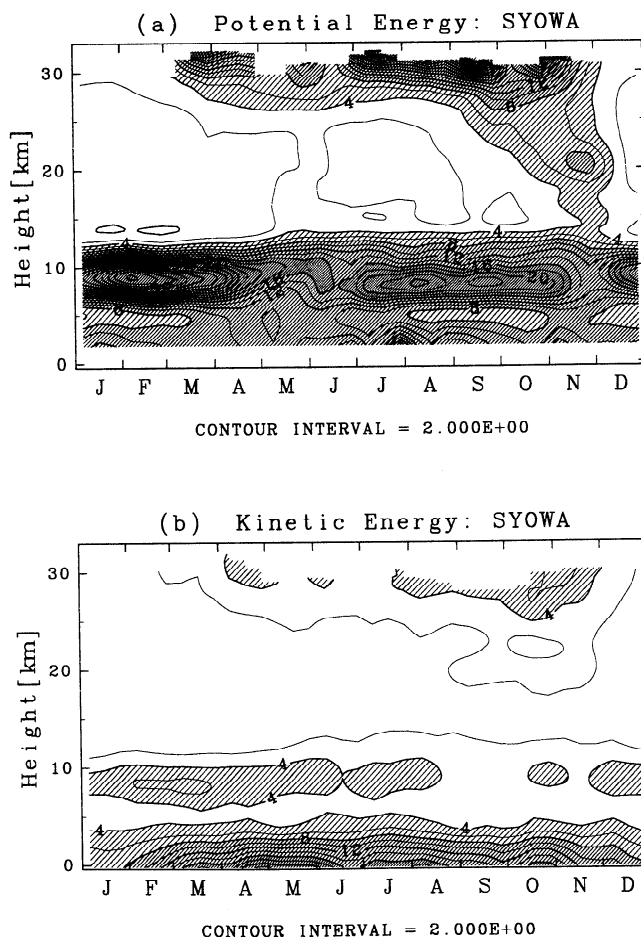
(a)   Potential Energy: SYOWA

CONTOUR INTERVAL = 2.000E+00

(b)   Kinetic Energy: SYOWA

CONTOUR INTERVAL = 2.000E+00

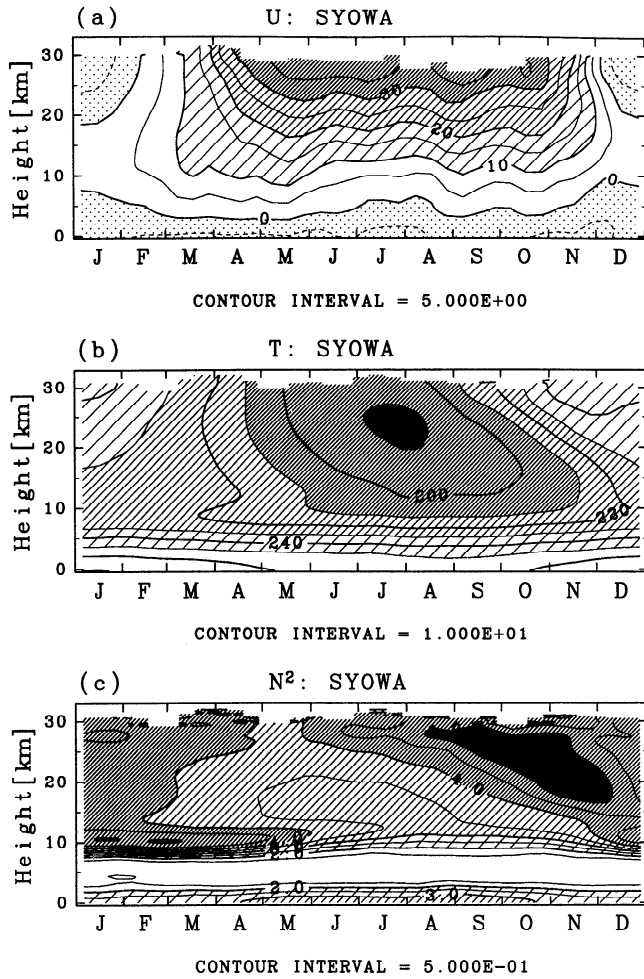**Figure 5.** The same as Figure 4 but for Syowa (69.0°S, 39.6°E).

Figure 6. A composite of the time-height section of (a) zonal wind u (m s^{-1}), (b) temperature T (K), and (c) Brunt-Väisälä frequency squared N^2 (10^{-4} s^{-2}) at Syowa. The contour intervals are 5 m s^{-1}, 10 K, and 5 × 10^{-5} s^{-2}, respectively.

clear. However, in the Antarctic, N^2 has a dramatic annual variation, being small in winter and large in spring. South of 60°S, the static stability is increased by ~20–60% when the springtime warming occurs. While N^2 in the Antarctic is smaller than at lower latitudes in winter, the relative magnitudes of N^2 reverse in spring. In spring the high-stability area appears earlier at 135°E, 60°S and propagates gradually to 45°W, 70°S over the South Pole in August to November. On the other hand, the region of high stability disappears simultaneously at all latitudes. The high stability-area remains longer in the 135°E sector than in the 45°W sector.

Figure 11 shows the latitude-time section of the potential energy of gravity waves, in which the Antarctic stations are projected onto the longitude lines of 135°E and 45°W. The position of each station is marked on the right side of the vertical axis. Note that the latitudes of the positions along this longitude line are not the same as the geographical latitudes of the stations. Solid boxes indicate the time and location of the maximum in static stability at the latitude in Figure 10. At most Antarctic stations a spring maximum in potential en-

ergy is clearly observed. The gravity wave energy enhancement does not occur simultaneously at all stations but rather coincides with the appearance of the stability maximum at each station. On the 135°E side of the diagram, although there is a delay of ~ 1 month between the static stability maximum and potential energy maximum, gravity wave energy grows through the period of high stability as shown by the shaded region of Figures 10 and 11. Furthermore, as the energy enhancement disappears almost simultaneously at all stations, the energy enhancement remains longer at stations in the 135°E sector. This is the same type of behavior as shown by the static stability distribution in Figure 10.

3.3. Estimates of Momentum Flux

Since the w component is not available from the radiosonde data, estimates of momentum fluxes were obtained by the method proposed by *Vincent et al.* [1997] assuming the "universal" gravity wave spectrum. The details of the method are described as follows.

For a monochromatic wave the upward flux of zonal momentum $\overline{u'w'}$ is expressed as

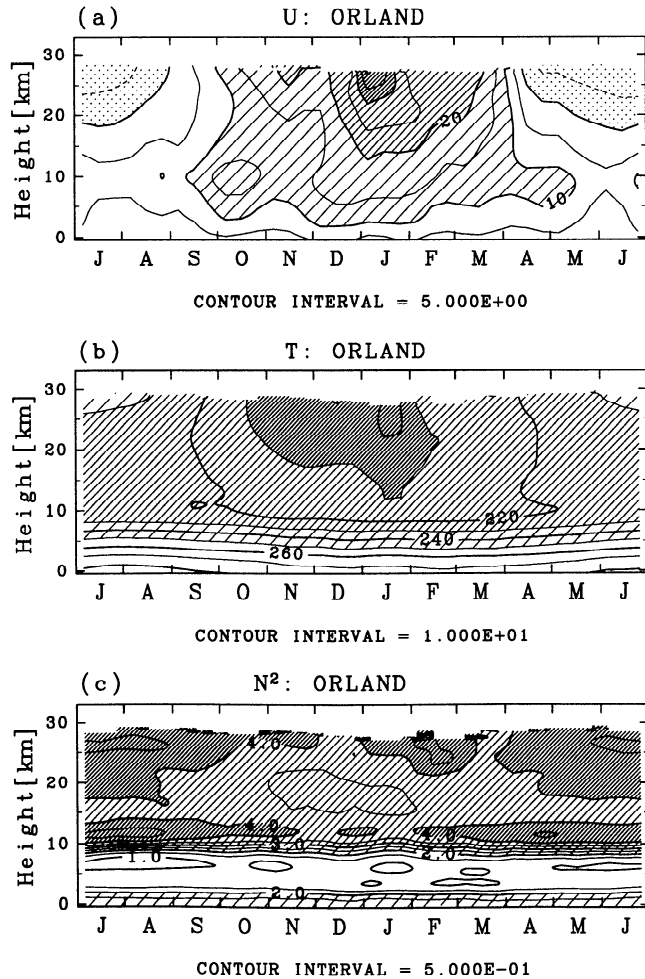$$\overline{u'w'} = -\frac{\hat{\omega}g}{N^2}\frac{\overline{u'T'_{+90}}}{\overline{T}},\tag{1}$$

Figure 7. The same as Figure 6 but for Orland.

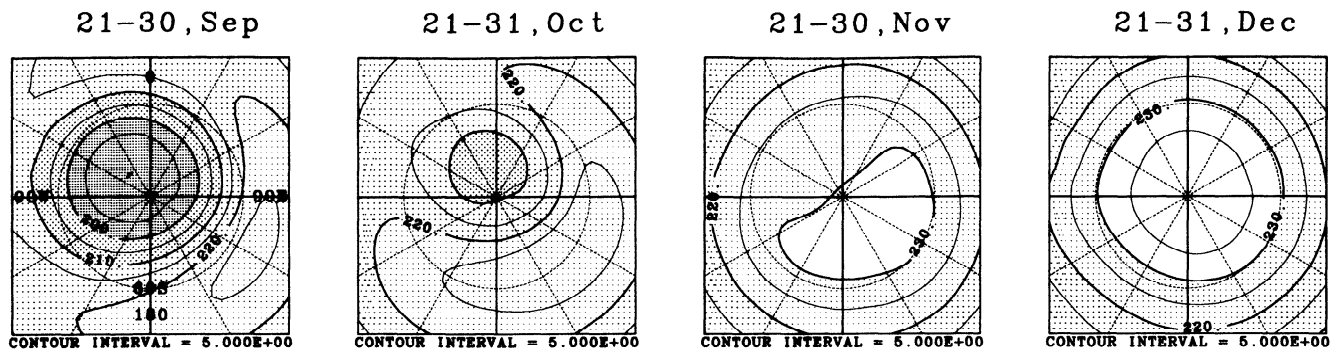## 21-30,Sep 21-31,Oct 21-30,Nov 21-31,Dec

Figure 8. Polar stereomap of temperature T (Kelvin) averaged over 10 years for each month at 50 hPa. The contour interval is 5 K. Darker shading is used for colder regions.

where T'_{+90} is defined as the temperature fluctuation whose phase is shifted downward by 90°, and $\hat{\omega}$ is the intrinsic frequency. As waves are not always monochromatic, the phase was shifted for every wavenumber component by use of the Hilbert transform. The intrinsic frequency $\hat{\omega}$ was replaced with $\bar{\omega}$, an average of $\hat{\omega}$ assuming the universal spectrum:

$$\bar{\omega} = \frac{\int_{|f|}^{N} \hat{\omega} B(\hat{\omega}) d\hat{\omega}}{\int_{|f|}^{N} \hat{\omega} d\hat{\omega}}, \tag{2}$$

where $B(\hat{\omega}) \equiv (p-1) f^{p-1} \hat{\omega}^{-p}$ is the normalized frequency spectrum of gravity wave energy. The parameter p was taken to be 2, the value indicated by many observations. Note that a few assumptions in addition to the use of a universal spectrum were used in this method. Temperature and horizontal wind fluctuations were all considered to be due to gravity waves. Only gravity waves propagating energy upward were considered. When gravity waves propagate energy downward, the sign of the estimated momentum flux is opposite to that of the true momentum flux.
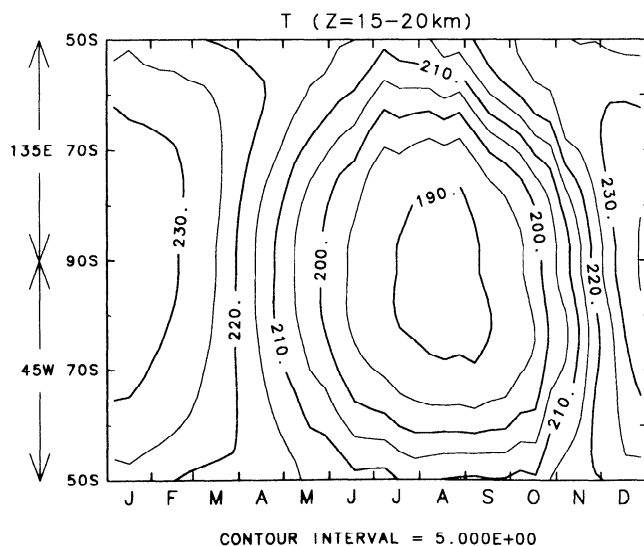
Estimation of momentum flux was made for the height region of 5–25 km. The background temperature $\bar{T}$ and Brunt-Väisälä frequency N were calculated at each height for each profile. Figures 12 and 13 show time-height sections of $\overline{u'w'}$ and $\overline{v'w'}$ calculated for Syowa in the Antarctic and Orland in the Arctic, respectively.

At Syowa, $\overline{u'w'}$ is negative and large from autumn to spring in the lower stratosphere. The meridional component $\overline{v'w'}$ is positive in winter, but the absolute value is smaller than that of $\overline{u'w'}$. This means that most gravity waves propagate westward relative to the background wind in this season. In summer, $\overline{u'w'}$ is weakly positive. The absolute value of $\overline{u'w'}$ from autumn to spring is only 20% of the statistical value in the winter lower stratosphere at midlatitude obtained by MST radar observations [e.g., Sato, 1994]. It is interesting that $\overline{u'w'}$ does not change vertically and there is no clear spring maximum as is observed in the potential and kinetic energies.

At Orland, $\overline{u'w'}$ is also negative and $\overline{v'w'}$ is positive in autumn to spring. The absolute values of $\overline{u'w'}$ are as large as
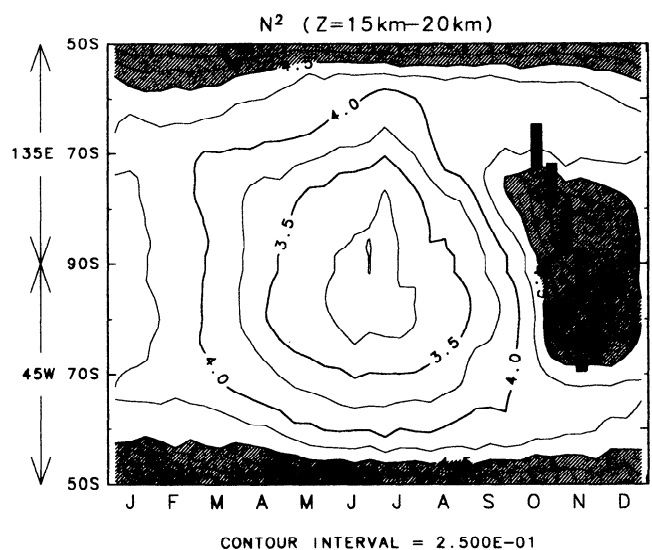

Figure 9. The latitude-time section of temperature (K) averaged over 10 years in the height region of 15–20 km in the Southern Hemisphere. The contour interval is 5 K.

Figure 10. The latitude-time section of Brunt-Väisälä frequency squared (10^{-4} s^{-2}) averaged over 10 years in the height region of 15–20 km in the Southern Hemisphere. Solid boxes denote the time when the static stability is highest at each latitude. The contour interval is 2.5×10^{-5} s^{-2}.

Potential Energy (Z=15km–20km)
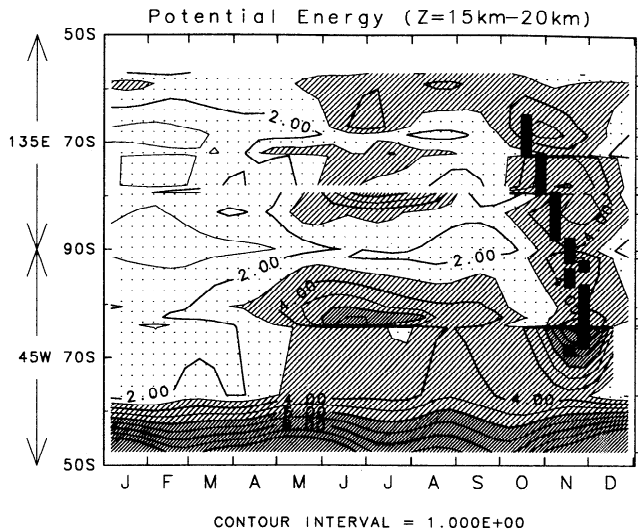

CONTOUR INTERVAL = 1.000E+00

Figure 11. The latitude-time section of potential energy averaged over 10 years in the height region of 15–20 km in the Southern Hemisphere. Solid boxes denote the times when the static stability is highest at each latitude (as in Figure 10). Regions of higher energy are shaded darker. The units are $m^2 \, s^{-2}$. The contour interval is 1 $m^2 \, s^{-2}$.

(a) u'w' : SYOWA

CONTOUR INTERVAL = 5.000E+00

(b) v'w' : SYOWA

CONTOUR INTERVAL = 5.000E+00

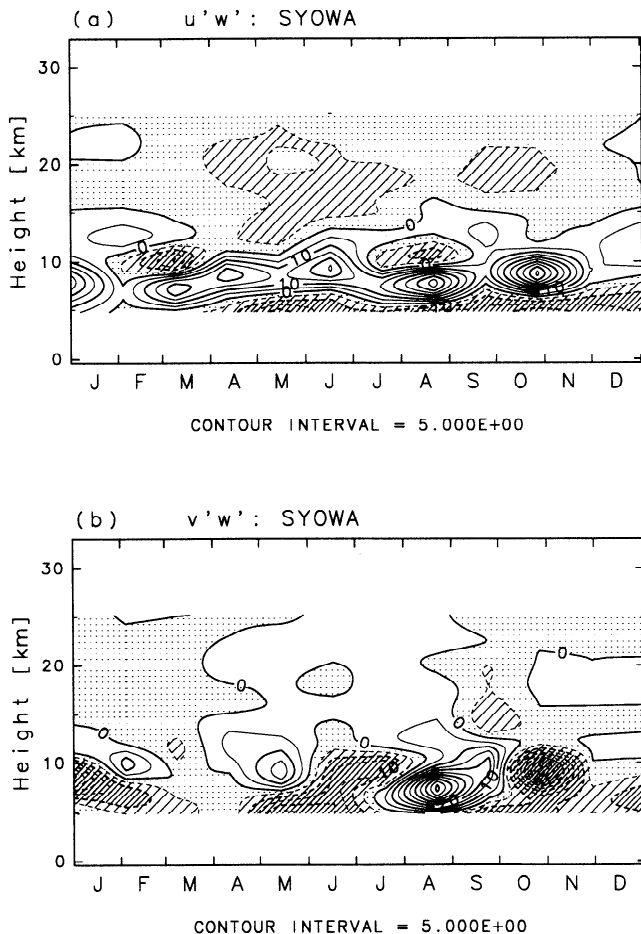**Figure 12.** The time-height section of (a) $\overline{u'w'}$ and (b) $\overline{v'w'}$ at Syowa. The contour interval is 5×10^{-3} $m^2 \, s^{-2}$. The regions of negative value are shaded.

(a) u'w' : ORLAND

CONTOUR INTERVAL = 5.000E+00

(b) v'w' : ORLAND
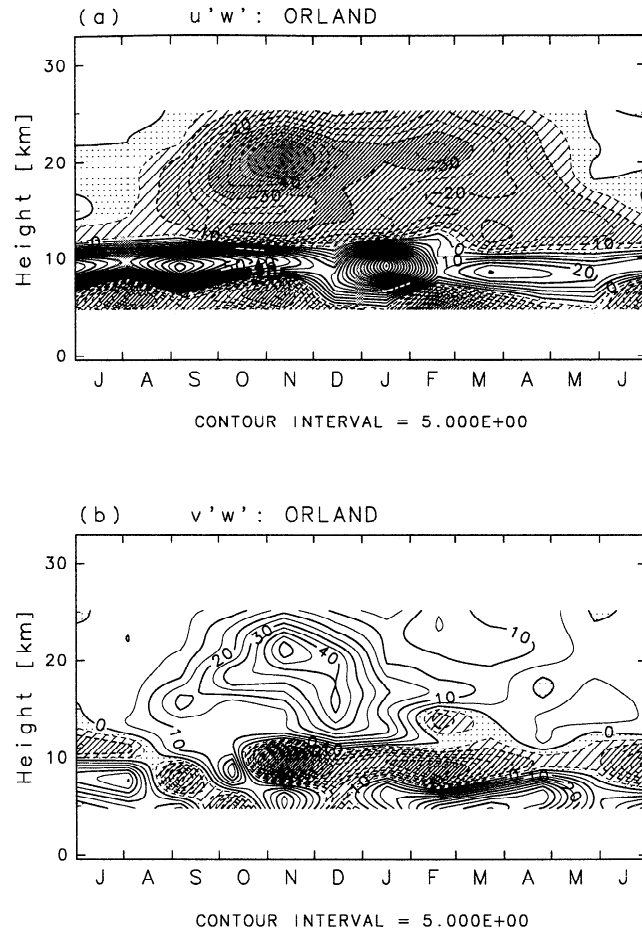

CONTOUR INTERVAL = 5.000E+00

Figure 13. The same as Figure 12 but for Orland.

those of $\overline{v'w'}$ in early winter. The absolute value of momentum flux in this season is much larger than that of Syowa and comparable to the statistical value obtained by *Sato* [1994]. This result suggests that most gravity waves propagate northwestward relative to the background wind. In summer, $\overline{u'w'}$ is weakly positive. The implications of this for wave propagation directions will be confirmed by a hodograph analysis in section 3.5. Further quantitative discussion is not made here, however, since this estimation method includes several unconfirmed assumptions.

3.4. Correlation between Gravity Wave Intensity and Background Wind

For the Arctic, gravity waves forced by topography have been investigated in many observational studies [e.g., *Chan et al.*, 1993]. In order to examine the source of gravity waves the correlation between the gravity wave intensity and the unfiltered wind speed $\sqrt{u^2 + v^2}$ was examined for Orland in the Arctic and Syowa and Casey in the Antarctic. Correlation coefficients were calculated for each season using the twice-daily data over 10 years. Kinetic energy $\overline{u'^2 + v'^2}$ was used as a measure of gravity wave intensity.

At first, to examine the possibility of an orographic source, the correlation between the surface wind speed averaged in the height region of 1-2 km and the gravity wave intensity
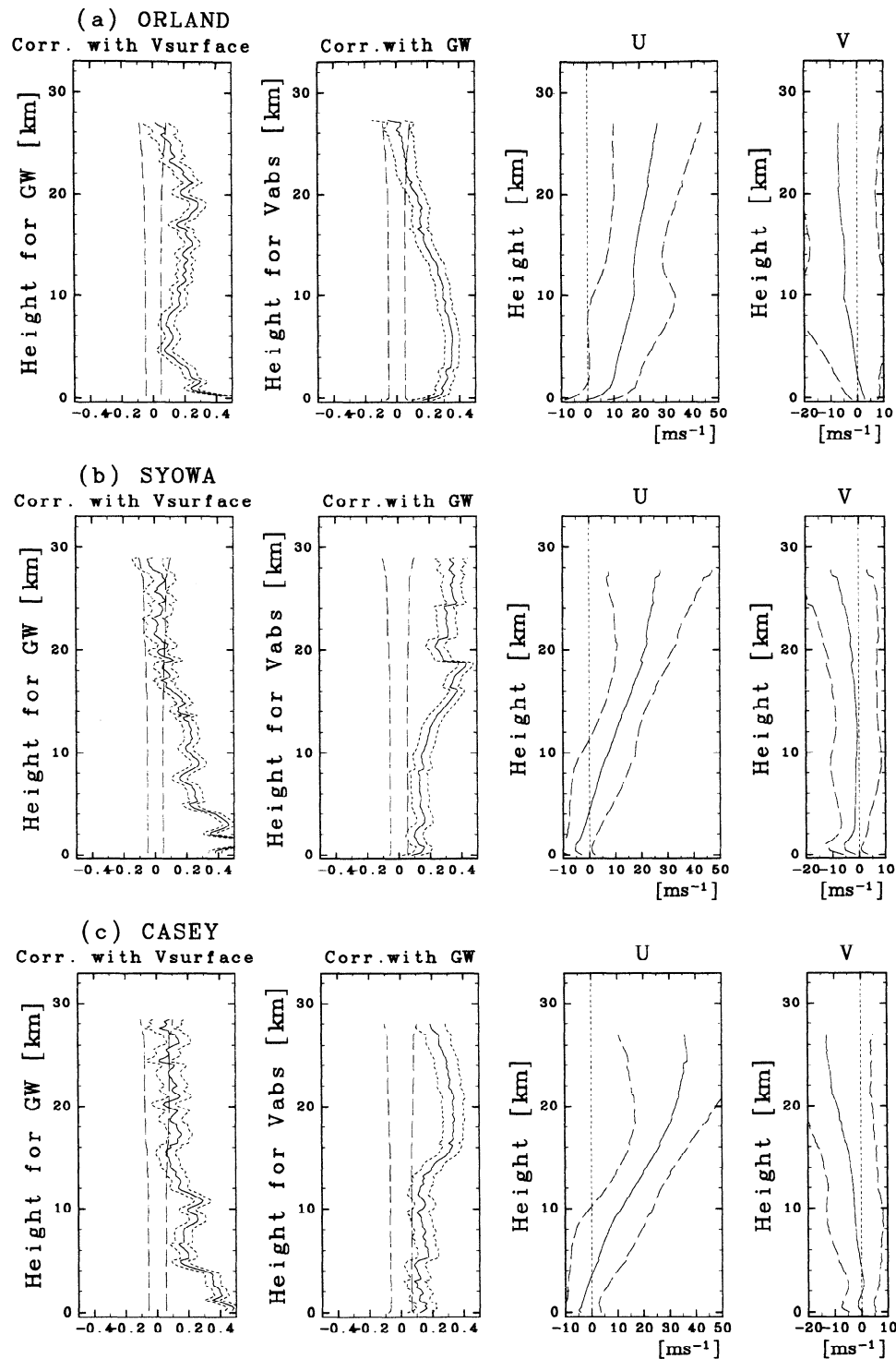
Figure 14. (First plots) Correlation between the surface background wind and kinetic energy of gravity waves at each height, (second plots) correlation between the kinetic energy in the height region of 15-20 km and background horizontal wind at each height, and (third plots) mean zonal wind and (fourth plots) meridional wind at each station. (a) Orland in winter (December–February), and (b) Syowa and (c) Casey in spring (September–November). In the first and second plots, thick curves show the correlation, short-dashed curves show the estimate bounds with the reliability of 95%, and long-dashed curves show the limits of significant correlation. In the third and fourth plots, the solid curves show the mean wind and the difference between dashed and solid curves shows standard deviation.

at each height was calculated. Results are shown in the first plots of Figure 14 for Orland in winter (December–February) and for Syowa and Casey in spring (September–November), when the gravity wave energy is large. The vertical axis

shows heights for the gravity wave intensity. The thick curve in each profile shows the correlation, and short-dashed curves show the 95% confidence limit. Long-dashed curves show the limits of significant correlation. At Orland the gravity
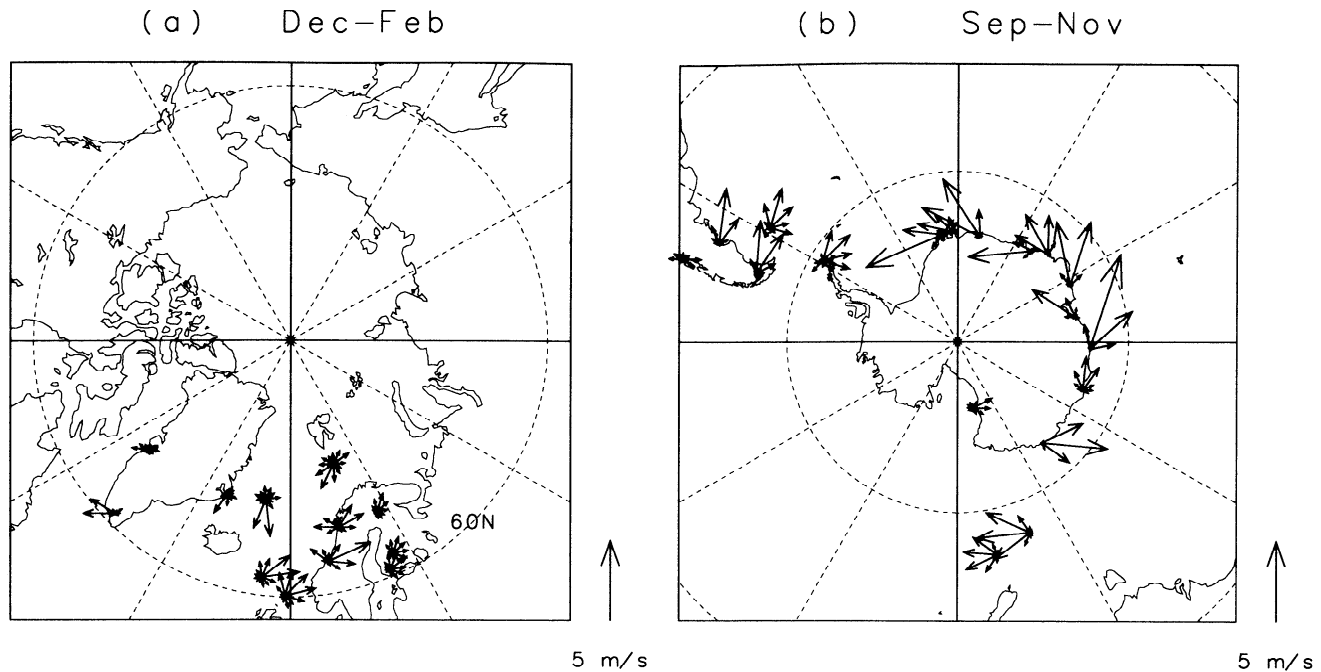
(a)   D e c — F e b   (b)   S e p — N o v

5 m/s   5 m/s

Figure 15. Wind speed (m s^{-1}) at z = 400 m weighted by probability density of the wind direction at each station in (a) the Arctic in winter and (b) the Antarctic in spring.

wave intensity in the height region between 15 and 20 km is highly correlated with the surface wind. On the other hand, the correlation at Syowa and Casey is not significant.

Next, the correlation between the gravity wave intensity averaged in the height region of 15–20 km, and the wind speed at each height was calculated for the same period at each station. The results are shown in the second plots of Figure 14. The line types are the same as for the first plots. The vertical axis shows wind speed heights.

At Orland the gravity wave intensity is highly correlated with the surface wind speed. In the lower stratosphere above a height of 15 km the correlation is low. In the Arctic, at most stations, in particular those with strong surface wind, gravity wave intensity is highly correlated with the surface wind speed. On the other hand, at Syowa and Casey the gravity wave intensity is highly correlated with the wind speed above 15 km, though the correlation with the surface wind is not high. Similar characteristics are observed at other Antarctic stations.

It should be noted that the surface wind at Syowa and Casey is easterly, while it is westerly at Orland (third and fourth plots of Figure 14). Since the mean wind in the lower stratosphere is westerly both in the Arctic in winter and in the Antarctic in spring, there is a critical level for topographically forced gravity waves at these Antarctic stations.

The above results suggest that the sources of gravity waves in the Arctic differ from those in the Antarctic. Gravity waves in the lower stratosphere at Orland are likely forced by topography, while sources of gravity waves at Syowa and Casey probably exist in the lower stratosphere.

Figure 15 shows the probability density of the wind direction at the 400 m height at each station. Results are shown for the Arctic in winter (December–February, Figure 15a) and the Southern Hemisphere in spring (September–November,

Figure 15b). The length of an arrow indicates wind speed weighted by the probability density of the wind direction. In the Arctic the surface wind is westerly at many stations. In the Southern Hemisphere, although the westerly wind is dominant in midlatitude (e.g., at stations near the Andes and at station U in Figure 1), the surface wind is easterly at most stations along the coast of Antarctica. This is due to katabatic winds from the interior of the continent [*König-Langlo et al.*, 1998; *Connolley and King*, 1993]. This distinctive feature of the mean wind creates a critical level for topographically forced gravity waves in the middle troposphere at most Antarctic stations.

3.5. Hodograph Analysis

In order to examine detailed gravity wave characteristics, such as energy propagation direction, wavelength, and frequency, the vertical variation of the horizontal wind vector (hodograph) was examined in the height region of 15–25 km. For a hydrostatic monochromatic inertia-gravity wave, horizontal wind fluctuations parallel to the wave number vector **k** (U') and perpendicular to the wave number vector (V') are expressed using the polarization relations of gravity waves as

$$U' = \text{Re}[\frac{\hat{\omega}kA}{\sqrt{\hat{\omega}^2 - f^2}} \exp i(mz + \phi_0)], \qquad (3)$$

$$V' = \text{Re}[\frac{-ifkA}{\sqrt{\hat{\omega}^2 - f^2}} \exp i(mz + \phi_0)], \qquad (4)$$

$$\frac{T'}{T} = \text{Re}[\frac{imA}{g} \exp i(mz + \phi_0)], \qquad (5)$$

(a) ORLAND(63.7N, 9.6E)

(b) SYOWA(69.0S, 39.6E)
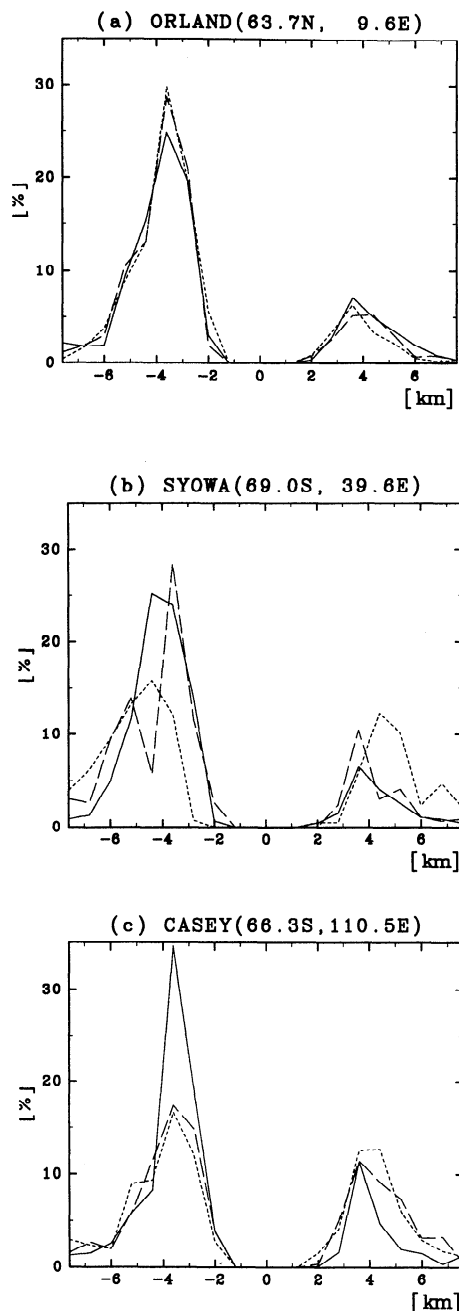

(c) CASEY(66.3S,110.5E)

Figure 16. Probability density of the vertical wavelength of gravity waves at (a) Orland (63.7°N, 9.6°E), (b) Syowa (69.0°S, 39.6°E) and (c) Casey (66.3°S, 110.5°E). Positive and negative values mean that gravity waves propagate energy downward and upward, respectively. The solid curves show the average for the time period from December to February, short-dashed curves show the average for June to August, and the long-dashed curves show the average for September to November.

where f is the Coriolis parameter, i is the imaginary unit, Re[ ] denotes the real part of a complex, k is horizontal wavenumber, m is vertical wavenumber, z is altitude, A is a constant for amplitude, and ϕ_0 is a constant phase at $z = 0$. Equations (3) and (4) indicate that clockwise (counterclockwise) hodograph rotation with height in the Northern

(Southern) Hemisphere means upward energy propagation of gravity waves [*Hirota and Niki*, 1985].

As the quality of temperature data is usually expected to be better than that of horizontal wind data, temperature fluctuations were used to determine vertical wavenumber m as a first step. A least squares fitting with a fixed vertical wavelength was applied to temperature fluctuations for every 3 km height interval in the height region of 15–25 km. Using 61 fittings of different vertical wavelength in a range of 2.0–8.0 km with an interval of 0.1 km, the vertical wavenumber m and the phase constant $\phi_0 = \phi_T$ with the least residual were obtained.

Next, a low-pass filter with a cutoff length of 2 km was applied to the interpolated u, v data. The band-pass-filtered wind data were not used to avoid contamination by the background wind in case of large vertical shear. A least squares fitting for the low-pass-filtered u and v values was performed to the form of superposition of a linear background and a sinusoidal wave whose vertical wavenumber m was determined from temperature data. If the fluctuations are due to internal gravity waves, the phase constant ϕ_T should agree with that derived from the horizontal wind fluctuations ϕ_V. Thus wave parameters were estimated only when $|\phi_T - \phi_V|$ was < 0.5 rad ($\sim 30°$). The intrinsic frequency $\hat{\omega}$ was assumed to be positive without loss of generality. The statistics were made for cases in which the ratio of the short to the long axis of the ellipse was in the range of 0.2–0.9 and the kinetic energy was > 2 m^2 s^{-2}. The restricted oblateness of the ellipse meant that the intrinsic frequency $\hat{\omega}$ ranged between $10/9f$ and $5f$. Assuming the universal spectrum introduced in section 3.3, 70% of gravity wave energy was included in the statistics. Note that linearly polarized waves were excluded from the statistics.

Figure 16 shows the probability density as a function of vertical wavelength $\lambda_z \equiv 2\pi/m$ at Orland (63.7°N, 9.6°E), Syowa (69.0°S, 39.6°E), and Casey (66.3°S, 110.5°E). Positive and negative values of the vertical wavelength mean that gravity waves propagate energy downward and upward, respectively. The solid curve shows the average from December to February, whereas the short-dashed curve shows the average from June to August. The long-dashed curve shows the average from September to November when the gravity wave energy is maximized in the Antarctic. The dominant vertical wavelength of the observed gravity waves is $\sim$ 4 km, which reflects the transfer function of the band-pass filter used here. In general, gravity waves propagating energy upward dominate throughout the year at all stations. It is important, however, that a relatively large percentage of downward energy propagation is observed for July to August at Syowa and Casey and for September to November at Casey. Gravity waves carrying energy downward are $\sim$ 36–40% of all at these times, whereas they usually are $< 20\%$.

Figure 17 shows the probability density as a function of horizontal direction of propagation relative to the mean wind at each station in the Arctic in winter (December–February, Figure 17a), the Antarctic in winter (June–August, Figure 17b) and the Antarctic in spring (September–November, Figure 17c). The length of the arrow at each station indicates the probability density of the propagation direction. When the probability density is < 7 %, the arrow is omitted. The
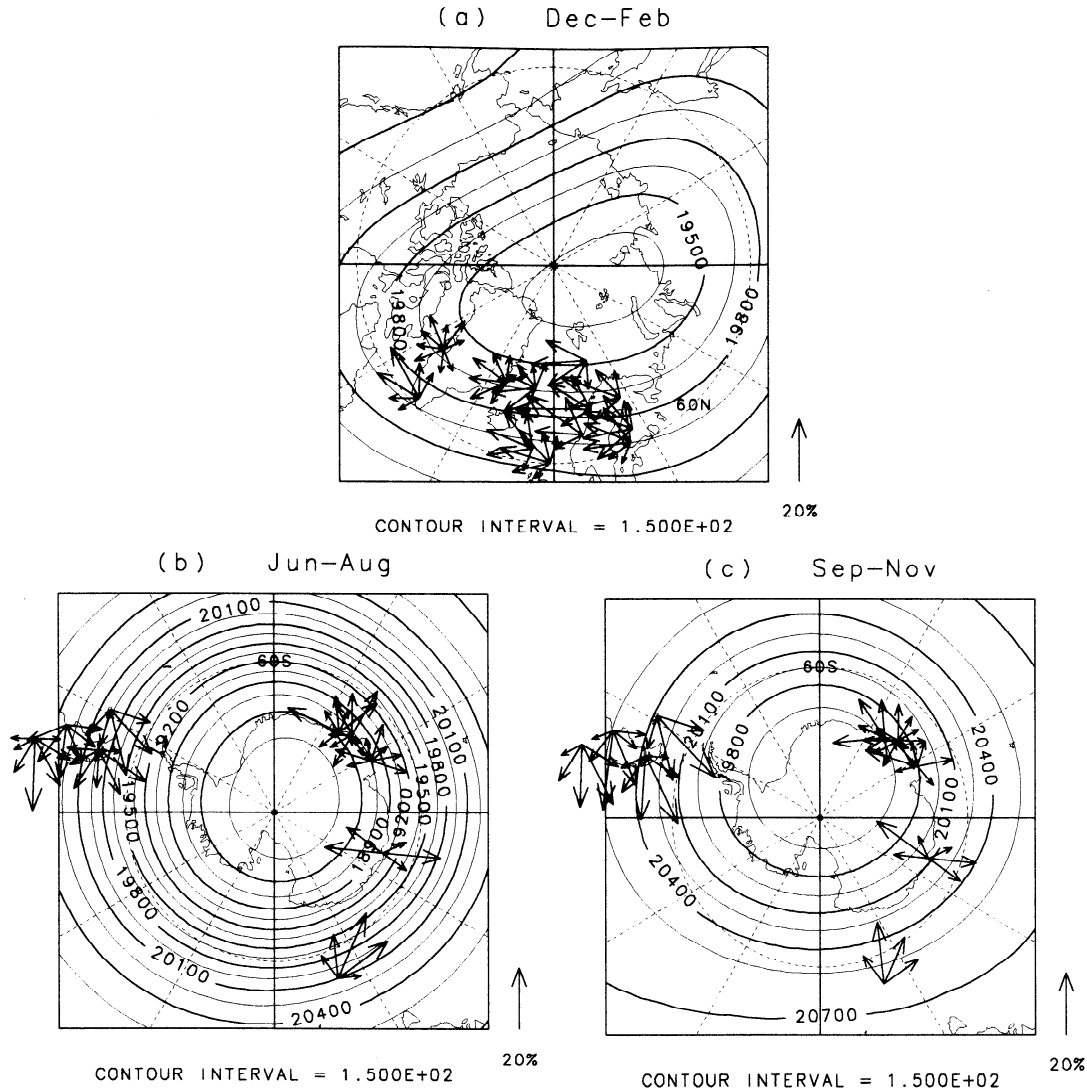
Figure 17. Horizontal direction of gravity wave propagation relative to the mean wind in (a) the Arctic in winter, (b) the Antarctic in winter, and (c) the Antarctic in spring. The length of each arrow shows the probability density of the wind direction at each station. The geopotential height (in m) at 50 hPa averaged over 10 years is also shown. The contour interval is 150 m.

contour lines in Figure 17 show the geopotential height at 50 hPa ($\sim$ 20 km) averaged over 10 years in each season to show the location and shape of the polar vortex. Results for stations in which fewer meaningful estimates of wave parameter were obtained are not shown in Figure 17.

In the Arctic the geopotential height shows that a strong polar vortex in winter is deformed by stationary planetary waves. Most meteorological stations analyzed in this study are located at the edge of the polar vortex, where gravity waves propagate westward relative to the mean wind. In the Antarctic in winter the polar jet is zonally symmetric and stronger than that in the Arctic in winter. At midlatitude in both the South American sector and of station U at 160°W, gravity waves propagating westward relative to the mean wind are dominant. However, at stations on the coast of Antarctica inside the vortex, a large range in propagation direction is seen. In particular, it is interesting that gravity waves propagate both southward and northward at Casey. In

spring, although the polar vortex begins to shift toward the direction of 45°W, it is still strong compared with that in the Arctic. The direction of propagation in spring is basically similar to that in winter.

It seems that the difference in dominant directions of gravity wave propagation is related to the difference in the surface winds. As shown in section 3.4, the surface wind is westerly at most Arctic and Southern Hemisphere midlatitude stations, while it is easterly at the Antarctic stations. The horizontal direction of wave propagation is very large at the Antarctic stations, where easterly surface winds dominate.

As introduced in section 1, the ground-based phase velocity of gravity waves is important because dissipation of gravity waves can accelerate or decelerate the background wind to a value approaching that of the ground-based phase velocity. The probability densities of ground-based phase velocity and background wind speed are shown in Figure 18 for Orland in winter and for Syowa and Casey in spring. In Fig-
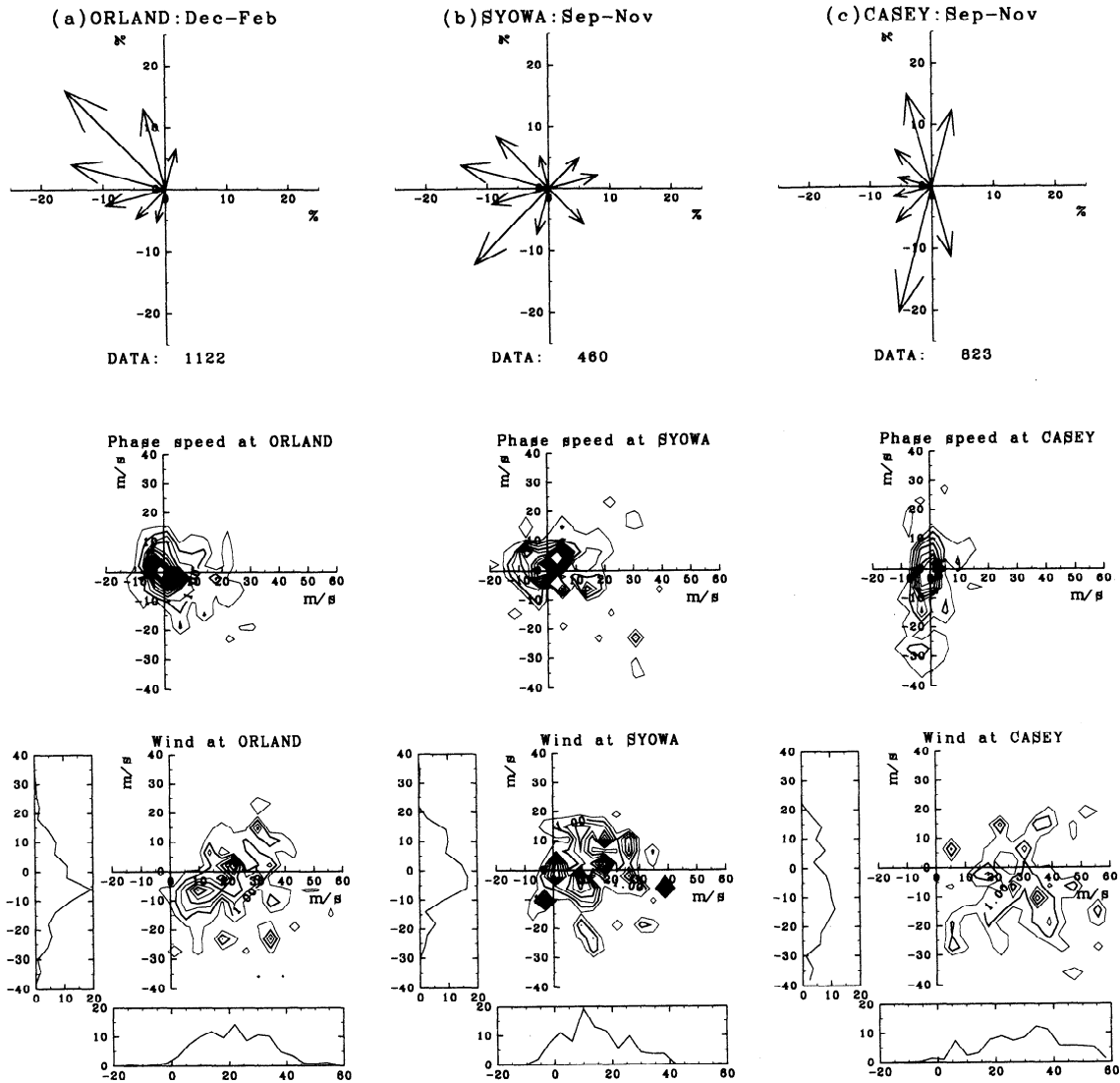
Figure 18. Probability density of the (top) horizontal direction of wavenumber vector, (middle) ground-based phase velocity, (bottom) and background horizontal wind at (a) Orland in winter and (b) Syowa and (c) Casey in spring, respectively. The length of each arrow in the Figure 18 (top) shows the probability density at the direction. The contour interval of Figure 18 (middle) and 18 (bottom) is 0.5 %.

ure 18 (top), the probability density of the horizontal direction of gravity wave propagation relative to the background wind (already shown in Figure 17) is presented for comparison. In Figure 18 (middle) the frequency distribution of ground-based phase velocity vectors is shown as a contour map. The ground-based phase velocity is defined by

$$c = (\widehat{\omega} + U \cdot k)\frac{k}{|k|^2}. \tag{6}$$

The absolute value of horizontal wavenumber k is estimated by the dispersion relation of hydrostatic gravity waves:

$$k^2 = \frac{\widehat{\omega}^2 - f^2}{N^2}m^2. \tag{7}$$

The probability density of the horizontal wind speed is shown in Figure 18 (bottom).

At Orland, gravity waves propagate northwestward relative to the background wind. As the mean wind is eastward, gravity waves propagate upstream. The probability density of ground-based phase velocity vectors is concentrated around zero. Absolute values of the ground-based phase velocity range from zero to 10 m s^{-1}.

At Syowa, gravity waves propagate westward relative to the background wind. This direction is also opposite to the background wind. However, the variability of the relative horizontal wind directions is larger than at Orland. The ground-based phase velocity is distributed largely around zero and extends slightly toward the northeast. The absolute values of the ground-based phase velocity are ~ 0–10 m s^{-1}. At Casey, gravity waves propagate southward and northward relative to the background wind. The probability density of ground-based phase velocity has a peak around zero. Besides, southward ground-based phase velocities are

also observed. Magnitudes of the ground-based phase speeds lie between 0 and 20 m s^{-1}.

4. Discussion

4.1. Enhancement of Gravity Wave Energy in Spring Over the Antarctic

In section 3.1, potential and kinetic energies of gravity waves are seen to be large in spring in the Antarctic. This seasonal variation is remarkable and not seen at midlatitudes in both hemispheres or in the Arctic. On the other hand, the spring maximum of the momentum flux is not clear in the Antarctic. Here we discuss the meaning of the energy enhancement in spring and the difference in the seasonal variation between energy and momentum flux in the Antarctic.

It was shown in section 3.2 that the spring maximum of gravity wave energy in the Antarctic seems to be strongly related to high static stability. A similar spring maximum is seen at the South Pole [*Pfenninger et al.*, 1999]. The position relative to the polar night jet is different between the South Pole and the coastal stations examined in this study, and hence the seasonal variation of the background wind is different. Thus we confirm that the gravity wave energy enhancement in spring is mainly affected by the static stability rather than the background wind. This influence may be attributed to the following processes: gravity wave saturation, modification of the wave structure, or shift in the location of the polar vortex.

The amplitude of gravity waves is restricted not only by dissipation or radiation relaxation but by local instability due to the wave wind or temperature fluctuations. When the local stability is neutral (i.e., sum of background static stability N and fluctuations of stability due to gravity waves is zero), gravity waves are called saturated. The amplitude of such saturated gravity waves depends on the Brunt-Väisälä frequency N. *Smith et al.* [1987] showed that the power spectral density of horizontal wind fluctuations for saturated gravity waves can be described by $F(m) = N^2/6m^3$ assuming $\Delta m \propto m$, where Δm is the band width in m space occupied by a gravity wave with vertical wavenumber m. This spectrum accords well with the observations. The saturated spectrum for potential energy divided by atmospheric density becomes $N^2/10m^3$. Thus potential energy is proportional to N^2 if gravity waves in the wavenumber band analyzed in this study are saturated.

It is also possible that the amplitudes of gravity waves are modified by the change in background static stability even when there are no dissipation processes. For example, the vertical component of group velocity for a linearly polarized gravity wave is described as $c_{gz} = -\hat{\omega}^2/kN$. Hence c_{gz} decreases when gravity waves approach the high-stability region. Assuming steady waves in a homogeneous atmosphere but with a slowly varying Brunt-Väisälä frequency N in the vertical, wave action density $E/\hat{\omega}$ is described as

$$\frac{d}{dz}(c_{gz}\frac{E}{\hat{\omega}}) = 0, \qquad (8)$$

so that $c_{gz}E/\hat{\omega}$ equals a constant [*Andrews et al.*, 1987]. Therefore wave action density increases in high-stability re-

gions where c_{gz} decreases. Because $\hat{\omega}$ is conservative in the assumed condition, gravity wave energy is proportional to the wave action and thus increases in high-stability regions.

A third possible energy enhancement mechanism may involve more intense generation of gravity waves by some mechanisms related to the springtime warming of the stratosphere. Propagation of the high-stability area in the spring Southern Hemisphere is attributed to the shift of the polar vortex. It is possible that the shear and/or the deceleration of the polar vortex affect the generation of gravity waves in spring. The absence of a clear spring maximum in momentum flux may be because momentum fluxes of opposite sign cancel each other out. In fact, the propagation direction at Syowa does have a larger variety than that at Orland.

4.2. Sources of Gravity Waves

At Orland in the Arctic the gravity wave intensity in the lower stratosphere is well correlated with the surface wind (Figure 14). Gravity waves propagate upstream, and the ground-based phase velocity is mostly zero (Figure 18). These facts strongly suggest that the gravity waves observed at Orland are forced by topography.

Ground-based phase speeds at Syowa are mostly zero, similar to that at Orland. However, they are not likely to be due to mountain waves because there is a critical level in the height region of 4-5 km (see Figure 14). Low correlation between gravity wave intensity and the surface wind supports this inference. At most coastal stations in the Antarctic the surface wind is commonly easterly, and there is a level with zero wind speed which corresponds to a critical level for topographically forced waves. Therefore it is natural to attribute the source of gravity waves in the Antarctic to the stratosphere.

Recently, *Sato et al.* [1999] examined the global characteristics of gravity waves using a high-resolution general circulation model. The bottom boundary condition of the model is that of an aqua planet. Thus there are no topographically forced gravity waves. In their model, gravity waves propagating energy downward are dominant around the polar night jet. They suggested that the polar jet is a possible source of the gravity waves.

The hodographs of the horizontal wind fluctuations examined in this study indicate the dominance of upward energy propagation. However, in the Antarctic the percentage of downward energy propagation in winter is relatively large. This is also consistent with the inference that the polar jet is a possible source of gravity waves in the stratosphere over Antarctica.

5. Concluding Remarks

Gravity waves in the Antarctic and Arctic lower stratosphere were examined based on operational radiosonde observation data gathered at 33 stations over the 10 year period between 1987 and 1996. The statistical characteristics of gravity waves in the Arctic and in the Antarctic are summarized as follows.

1. Both potential and kinetic energies of gravity waves vary annually with both showing maxima in winter in the Arctic and in spring in the Antarctic.

2. At most Antarctic stations the region with large gravity wave energy in spring propagates downward following the movement of the high-static stability region. Horizontally, the high-stability area moves gradually from 135°E, 50°S to 45°W, 70°S through the South Pole in spring. The gravity wave energy enhancement coincides with the stability maximum at each station.

3. The vertical flux of zonal momentum is mostly negative and large in winter in both hemispheres, indicating the dominance of gravity waves propagating westward relative to the mean wind. The spring maximum as observed in gravity wave energy in the Antarctic is not clear in the profile of momentum flux.

4. High correlation is observed between gravity wave energy in the lower stratosphere and the mean surface wind at most Arctic stations. On the other hand, at most stations in Antarctica, gravity wave energy in the stratosphere is positively correlated with the stratospheric mean wind speed.

5. Hodograph analysis in the vertical suggests that gravity waves propagating energy upward are dominant in both hemispheres. The percentage of downward propagation increases in winter and spring in the Antarctic stations. Gravity waves propagating westward relative to the mean wind dominate in the Arctic, while the dominant direction of gravity wave propagation varies from station to station in the Antarctic.

Taking advantage of operational data with broad temporal-spatial coverage and consisting of simultaneous observations of temperature and horizontal wind speeds, we have identified unique seasonal variations and structures of gravity waves at the Antarctic and the Arctic stations. Further analysis of the physical mechanism causing these characteristics is necessary.

In this study, we have concentrated on gravity waves with vertical wavelength of 2–8 km because of the limited vertical sampling intervals of the data. However, gravity waves with shorter vertical wavelengths may also be important. In order to make a more quantitative analysis using the original high-resolution radiosonde data, *Pfenninger et al.* [1999] examined the vertical wavenumber spectrum of temperature and horizontal wind fluctuations at the South Pole and found a unique form of wave spectrum. Further analysis at other Antarctic stations is also needed.

We found an interesting increase in the energy of gravity waves above the heights of 27 km. To investigate this further, it is important to analyze the characteristics of gravity waves around and above this height region. For this purpose, techniques with wider coverage in height, such as rocket and/or satellite methods are useful.

References

Allen, S. J., and R. A. Vincent, Gravity wave activity in the lower atmosphere: Seasonal and latitudinal variations, *J. Geophys. Res.*, *100*, 1327–1350, 1995.

Andrews, D. G., J. R. Holton, and C. B. Leovy, *Middle Atmosphere Dynamics*, 489 pp., Academic, San Diego, Calif., 1987.

Bacmeister, J. T., M. R. Shoeberl, L. R. Lait, P. A. Newman, and B. Gary, Small-scale waves encountered during AASE, *Geophys. Res. Lett.*, *17*, 349–352, 1990.

Cariolle, D., S. Muller, F. Cayla, and M. P. McCormick, Mountain waves, polar stratospheric clouds, and the ozone depletion over Antarctica, *J. Geophys. Res.*, *94*, 11,233–11,240, 1989.

Carslaw, K. S. et al., Increased stratospheric ozone depletion due to mountain-induced atmospheric waves, *nature*, *391*, 675–678, 1998.

Chan, K. R., L. Pfister, T. P. Bui, S. W. Bowen, J. Dean-Day, B. L. Gary, D. W. Fahey, K. K. Kelly, C. R. Webster, and R. D. May, A case study of the mountain lee wave event of January 6, 1992, *Geophys. Res. Lett.*, *20*, 2551–2554, 1993.

Connolley, W. M., and J. C. King, Atmospheric water-vapour transport to Antarctica inferred from radiosonde data, *Q. J. R. Meteorol. Soc.*, *99*, 325–342, 1993.

Dunkerton, T. J., The role of gravity waves in the quasi-biennial oscillation, *J. Geophys. Res.*, *102*, 26,053–26,076, 1997.

Hirota, I.,and T. Niki, A statistical study of inertial gravity waves in the middle atmosphere, *J. Meteorol. Soc. Jpn.*, *63*, 1055–1066, 1985.

Kitamura, Y., and I. Hirota, Small-scale disturbances in the lower stratosphere revealed by daily rawin sonde observations, *J. Meteorol. Soc. Jpn.*, *67*, 817–831, 1989.

König-Langlo, G., J. C. King, and P. Pettre, Climatology of the three coastal Antarctic stations Dumont d'Urville, Neumayer, and Halley, *J. Geophys. Res.*, *103*, 10,935–10,946, 1998.

Lindzen, R. S., Turbulence and stress owing to gravity wave and tidal breakdown, *J. Geophys. Res.*, *86*, 9,707–9,714, 1981.

Maruyama, T., Upward transport of westerly momentum due to disturbances of the equatorial lower stratosphere in the period range of about 2 days–A Singapore data analysis for 1983–1993, *J. Meteorol. Soc. Jpn.*, *72*, 423–432, 1994.

Matsuno, T., A quasi one-dimensional model of the middle atmosphere circulation interacting with internal gravity waves, *J. Meteorol. Soc. Jpn.*, *60*, 215–226, 1982.

Murayama, Y., T. Tsuda, and S. Fukao, Seasonal variation of gravity wave activity in the lower atmosphere observed with the MU radar, *J. Geophys. Res.*, *99*, 23,057–23,069, 1994.

Pfenninger, M., A. Z. Liu, G. C. Papen, and C. S. Gardner, Gravity wave characteristics in the lower atmosphere at South Pole, *J. Geophys. Res.*, *104*, 5963–5984, 1999.

Phillpot, H. R., Antarctic stratospheric warming reviewed in the light of 1967 observations, *Q. J. R. Meteorol. Soc.*, *95*, 329–348, 1969.

Phillpot, H. R., A note on some early radiosonde temperature observations in the Antarctic lower stratosphere, *Pure Appl. Geophys.*, *130*, 171–180, 1989.

Sato, K., A statistical study of the structure, saturation and sources of inertia-gravity waves in the lower stratosphere observed with the MU radar, *J. Atmos. Terr. Phys.*, *56*, 755–774, 1994.

Sato, K., and T. J. Dunkerton, Estimates of momentum flux associated with equatorial Kelvin and gravity waves, *J. Geophys. Res.*, *102*, 26,247–26,261, 1997.

Sato, K., F. Hasegawa, and I. Hirota, Short-period disturbances in the equatorial lower stratosphere, *J. Meteorol. Soc. Jpn.*, *72*, 859–872, 1994.

Sato, K., T. Kumakura, and M. Takahashi, Gravity waves appearing in a high-resolution GCM simulation, *J. Atmos. Sci.*, *56*, 1005–1018, 1999.

Smith, S. A., D. C. Fritts, and T. E. VanZandt, Evidence for saturated spectrum of atmospheric gravity waves, *J. Atmos. Sci.*, *44*, 1404–1410, 1987.

Vincent, R. A., S. J. Allen, and S. D. Eckermann, Gravity-wave parameters in the lower stratosphere., in *Gravity Wave Processes – Their Parameterization in Global Climate Models*, edited by K. Hamilton, *NATO ASI Ser.,Ser. I*, 50, 7–25, 1997.

Whiteway, J. A. and T. J. Duck, Evidence for critical level filtering

of atmospheric gravity waves, *Geophys. Res. Lett., 23*, 145-148, 1996.

Whiteway, J. A, T. J. Duck, D. P. Donovan, J. C. Bird, S. R. Pal, and A. I. Carswell, Measurements of gravity wave activity within and around the Arctic stratospheric vortex, *Geophys. Res. Lett., , 24*, 1387-1390, 1997.

K. Sato, National Institute of Polar Research, Tokyo 173-8515, Japan.

M. Yoshiki, Department of Geophysics, Faculty of Science, Kyoto University, Kyoto 606-8502, Japan. (yoshiki@kugi.kyoto-u.ac.jp)